Chemical Engineering Journal 407 (2021) 128013

Contents lists available at ScienceDirect

Chemical Engineering Journal

journal homepage: www.elsevier.com/locate/cej

Kinetic modeling of dynamic changing active sites in a Mars-van Krevelen type reaction: Ethylene oxychlorination on K-doped $CuCl_2/Al_2O_3$

Hongfei Ma [a], Erling S. Sollund [a], Wei Zhang [a], Endre Fenes [a], Yanying Qi [a], Yalan Wang [a], Kumar R. Rout [a,b,*], Terje Fuglerud [c], Marco Piccinini [d], De Chen [a,*]

[a] Department of Chemical Engineering, Norwegian University of Science and Technology, Sem sælands vei 4, 7491 Trondheim, Norway
[b] Sintef Industry, Sem sælands vei 2A, 7491 Trondheim, Norway
[c] INOVYN, Herøya Industrial Park, 3936 Porsgrunn, Norway
[d] INOVYN, Rue Solvay 39, 5190 Jemeppe sur Sambre, Belgium

ARTICLE INFO

Keywords:
$CuCl_2/\gamma$-Al_2O_3
Ethylene oxychlorination
Kinetic model
Mars–van Krevelen
Reaction mechanism

ABSTRACT

A kinetic model was developed by taking into account the dynamic nature of the active sites in Mars–van Krevelen type catalytic reactions to predict the evolution of the reactant and product composition in the gas phase and the $CuCl_2$ concentration in the solid catalyst. The kinetic model at the steady-state of ethylene oxychlorination was obtained by combining transient experiments of the two half-reactions in the redox cycle, namely $CuCl_2$ reduced to CuCl by ethylene and CuCl oxidation by oxygen on the K-promoted $CuCl_2/\gamma$-Al_2O_3 catalyst. The dynamic transitions between $CuCl_2$ and CuCl of the active sites during the reactions are also modeled, and the contributions of two active sites, namely Cu coordination numbers of 4 and 3 in $CuCl_2$ were distinguished and included in the kinetic model. The kinetic models describe well the transient response of the reduction and oxidation steps as well as the reaction at the steady-state at different reaction conditions. Moreover, by combining the reactor modeling through a steady-state approach, the spatial-time resolved $CuCl_2$ profile and the C_2H_4 reaction rate can be well predicted in comparison with the experimental results. The approach of both transient and steady-state kinetic modeling and simulation is supposed to have general relevance for a better understanding of Mars–van Krevelen type reactions.

1. Introduction

The oxidation reaction is one of the most common and significant catalytic processes in the field of heterogeneous catalysis [1,2]. From the view of fundamental research, it is a good type of probe reaction to perform the reaction mechanism studies. On the other hand, in the view of industrial, many commercial catalytic processes are related to redox reactions, like NH_3-SCR, NO oxidation, ethylene oxychlorination, etc. [3–6], a better understanding of the mechanism in the process can furtherly improve the catalytic performance, which is closely related to costs and profits. All these reactions involve redox cycles where both reactants and catalysts undergo electron-transfer reactions through reduction and oxidation. For the oxidation reaction, the main reaction mechanism is the Mars–van Krevelen (MvK) mechanism [1,3,7–11], which besides the Langmuir–Hinshelwood (LH) and the Eley–Rideal (ER) mechanism are the most classical reaction mechanisms in heterogeneous catalysis [12,13]. In brief, the redox catalytic cycles can be simplified as Eqs. (1) and (2):

$$[CatO] + R - C \rightarrow RC - O + [Cat] \quad (1)$$

$$[Cat] + 0.5O_2 \rightarrow [CatO] \quad (2)$$

where [CatO] represents the oxidized catalyst surface and [Cat] is the reduced state. In a typical oxidation reaction, different states exist on the surface, the oxidized and free centers, as well as the adsorbed centers where the reactants and (or) products can be adsorbed. The characteristic feature of the MvK mechanism is that at least one component of the catalyst participates in the reaction of product formation, eventually making the components on the catalyst surface part of the reaction products [8,12]. In this mechanism, part of the catalyst surface is an active part and partakes in the reaction, one reactant forms a chemical bond with the surface, forming a thin layer of the metal–reactant bond [12]. The chemical state of the metal on the catalyst can be regenerated

* Corresponding authors at: Department of Chemical Engineering, Norwegian University of Science and Technology, Sem sælands vei 4, 7491 Trondheim, Norway (K.R. Rout and D. Chen).
E-mail addresses: kumarranjan.rout@sintef.no (K.R. Rout), de.chen@ntnu.no (D. Chen).

https://doi.org/10.1016/j.cej.2020.128013
Received 26 July 2020; Received in revised form 1 December 2020; Accepted 2 December 2020
Available online 8 December 2020

Nomenclature

List of Latin Symbols

A	Arrhenius frequency factor g_{Cu} mol^{-1} atm^{-1} s^{-1}
C	Concentration mol L^{-1}
C_p	Mass-based heat capacity J kg^{-1} K^{-1}
C_{Cl}	Cl concentration mol/g_{Cu}
C_{Cl^*}	Concentration at which 4-coordinated Cu was completely converted mol/g_{Cu}
$C_{Cl^{**}}$	Concentration at which the 3-coordinated Cu starts to form mol/g_{Cu}
C_{CuCl}	CuCl concentration mol/g_{Cu}
C_{CuCl^*}	The point of C_{CuCl^*} represents 2-coordinated Cu does not exist mol/g_{Cu}
$C_{CuCl^{**}}$	The starting point where the 2- and 3-coordinated Cu occur mol/g_{Cu}
C_{CuCl_2}	Reducible $CuCl_2$ concentration mol/mol_{Cu}
$C_{CuCl,max}$	Maximum concentration of CuCl mol/mol_{Cu}
d	Diameter m
d_e	The diameter of a sphere with the same surface to volume ratio as the particle
d_p	The diameter of a sphere with the same volume as the particle m
D_{AB}	Molecular diffusivity for A in a binary mixture of A and B m^2 s^{-1}
D	Diffusion coefficient m^2 s^{-1}
E_a	Activation energy kJ mol^{-1}
f	Friction factor –
j_A	Diffusive mass flux of species A kg m^{-1} s^{-1}
k	Reaction rate constant dep.
K_{eq}	O_2 Adsorption equilibrium constant atm^{-1}
m	Mass kg (or g)
n	Overall reaction order –
N	Molar quantity mol
p	Pressure Pa (or atm)
P	The emissivity of the catalyst particle –
P_e	Peclet number –
P_r	Prandtl number –
q	Heat flux W m^{-2}
Q	Radiations heat flux W m^{-2}
r	Radial coordinate m
r	Reaction rate mol g_{Cu}^{-1} s^{-1}
r_p	Radius of pellet m
R	The total volume-based reaction rate mol m^{-3} s^{-1}
Re	Reynold number –
R	Gas constant J K^{-1} mol^{-1}
s	Scalar –
Sc	Schmidt number –
S_F	Fractional selectivity –
t	Time s
T	Temperature K
$\bar{u}$	Superficial velocity m s^{-1}
U	Overall heat transfer coefficient W m^{-2} K^{-1}
V	Volume m^3
F	Volumetric flow rate ml/min
ω	Weighting factor –
X	Conversion %
z	Axial coordinate m
y	Molar ratio –

Greek Symbols

α	Heat transfer coefficient W m^{-2} K^{-1}
β	Coefficient depending on the particle geometry and packing density –
$\in$	Void fraction –
$\Delta_f H^0$	Heat of reaction kJ mol^{-1}
ΔG^0	Gibs free energy kJ mol^{-1}
ΔP	Pressure drop bar
λ	Thermal conductivity W m^{-1} K^{-1}
μ	Dynamic gas viscosity kg s^{-1} m^{-1}
μ_j	The chemical potential of species j –
ν	Stoichiometric coefficient –
ω	Mass fraction –
ϕ	Thiele modulus –
ρ	Total density kg m^{-3}
τ	Space-time/shear stress s Pa^{-1}
θ	Angular coordinate °
θ^*	The fraction of empty active sites –
θ	Coverage –
ξ	Extent of reaction mol

Subscripts

*	Adsorbed
+	Forward
−	Backward
A, B, C, D	Chemical compound
atm	Atmosphere
cal	Calculated
cat	Catalyst
eff	Effective
er	Effective radial
exp	Experimental
g	Gas
i	Inner
in	Initial/reactor inlet
o	Outlet
obs	Observation
out	Outside tube
par	Parameter
r	Radial coordinate
ref	Reference
s	The surface of the catalyst
sp	Specific
ss	Steady-state
v	Volume-based
w	Tube wall
0	Initial

Abbreviations and acronyms

BET	Brunauer–Emmett–Teller
BJH	Barrett–Joyner–Halenda
CN	Coordination number
EDC	Ethylene dichloride
ER	Eley–Rideal
ICP-OES	Inductively coupled plasma optical-emission spectrometry
KFM	Kubelka–Munk Function
LH	Langmuir–Hinshelwood
MS	Mass spectroscopy
MvK	Mars–van Krevelen
TPO	Temperature-programmed oxidation
TPR	Temperature-programmed reduction
UV–vis-NIR	Ultraviolet–visible and near-infrared spectroscopy
VCM	Vinyl chloride monomer
XRD	X-ray diffraction

by reacting with another reactant (s). The oxidation state of the catalysts and amount of vacancy (like O) can also affect the activity, selectivity, and stability. Many redox reactions involving C, Cl, N, and S follow a similar simplified mechanism on metal carbides, chlorides, nitrides, and sulfides [8]. These lattice components (O, S, Cl, H) participate in the formation of products lead to a relation of the catalytic activity. The active sites and the oxidation states are entirely dynamic and depending on the relative re-reduction and re-oxidation rates. And based on the fractional coverages, the surface state can be well described. However, due to the importance of redox reactions, an efficient method for predicting and controlling the catalytic cycles is still highly needed.

Ethylene oxychlorination (Eq. (3)) is the most important process to produce ethylene dichloride ($C_2H_4Cl_2$, EDC), the key intermediate used to produce vinyl chloride monomer (VCM) [5,14–22]. It was commonly reported that the ethylene oxychlorination reaction is catalyzed by a promoted $CuCl_2/\gamma$-Al_2O_3-based catalyst, and following the MvK mechanism, involving the reduction, oxidation, and hydrochlorination steps (Eqs. (4)–(6)) [14,15,23–33].

$$\text{Total reaction}: \quad C_2H_4 + 0.5O_2 + 2HCl \rightarrow C_2H_4Cl_2 + H_2O \tag{3}$$

$$\text{Reduction}: \quad 2CuCl_2 + C_2H_4 \rightarrow C_2H_4Cl_2 + 2CuCl \tag{4}$$

$$\text{Oxidation}: \quad 2CuCl + 0.5O_2 \rightarrow Cu_2OCl_2 \tag{5}$$

$$\text{Hydrochlorination}: \quad Cu_2OCl_2 + 2HCl \rightarrow 2CuCl_2 + H_2O \tag{6}$$

From the reaction mechanism, the chemical state of Cu transfers among $CuCl_2$, Cu_2OCl_2, and CuCl, and Cl is extracted by C_2H_4 with EDC formed as the product in the half-reaction and leaving Cl vacancy on the catalyst. The oxidation and hydrochlorination steps are dedicated to the regeneration of CuCl to $CuCl_2$. The oxidation state of Cu in the catalytic cycle at the steady-state reaction depends on the kinetic balance of the reduction, oxidation, and hydrochlorination steps. Based on the mechanism, CuCl is involved in the reaction cycle. However, it can be well known that the sublimation and aggregation of CuCl remain the commercial catalyst's challenges. Controlling CuCl concentration sufficiently low at the steady-state conditions is an efficient way to improve the stability of $CuCl_2/Al_2O_3$-based oxychlorination catalysts. Recently we systematically studied the mechanism of the catalytic cycle of ethylene oxychlorination on $CuCl_2/Al_2O_3$-based catalysts employing the operando Ultraviolet–visible and near-infrared spectroscopy (UV–vis-NIR) and monitored the $CuCl_2$ and CuCl evolution during the reaction [25,32,34]. It demonstrated that the oxidation state of Cu or Cl vacancy is highly dynamic, and changes with operating conditions and CuCl is dominating during the reaction on the neat $CuCl_2/Al_2O_3$ catalyst. The alkali metal, like K, is commonly used as the promoter in the $CuCl_2/Al_2O_3$-based catalyst to improve the catalytic performance, especially for the catalyst stability [24,31–33]. Both experimental and DFT results [35] suggest that KCl affects the redox properties of the Cu species, facilitating the regeneration of $CuCl_2$ from CuCl, and thus increasing the $CuCl_2$ concentration during the reaction. What is more, Muddada et al. [36] reported that by adding K into the $CuCl_2/Al_2O_3$-based catalyst, the byproduct formation was also prohibited by increasing the fraction of active Cu species and covering the exposed acid sites of the γ-Al_2O_3. Despite the importance of K promoter for the industrial oxychlorination catalysts, a quantitive model to predict the oxidation state and the catalytic behavior at various reaction conditions is still missing. Such a kinetic model is highly desired to improve our understanding of the effect of K on the catalytic cycle and provide guidelines for catalyst design, aiming to improve the catalyst performance.

Besides, process optimization in chemical industries requires precise knowledge of the reaction system. Several kinetic models of ethylene oxychlorination have been reported, mostly on the neat $CuCl_2/Al_2O_3$ catalyst [37–43]. A kinetic model for the K-promoted $CuCl_2/Al_2O_3$ catalyst is highly demanded, which is similar to the industrial ethylene oxychlorination catalysts. Besides, the reported kinetic models are mostly based on the Langmuir–Hinshelwood mechanism, and the changes in the Cu oxidation state with the operating conditions were not taken into account. Such a kinetic model has limited predictability in a wide range of operating conditions. Moreover, the oxidation state of Cu is the key parameter for predicting the catalyst stability. Therefore, a more reliable kinetic model with an accurate description of the reaction steps in the redox cycle is highly desired.

In the present work, we report an approach for developing a kinetic model of ethylene oxychlorination redox reaction by taking into account the dynamic changes of the active sites by means of combined transient and steady-state kinetic study. The proposed kinetic model can accurately describe the catalytic behaviors of the K-doped $CuCl_2/\gamma$-Al_2O_3 catalyst during the transient experiments of the half-reactions of reduction and oxidation steps. More importantly, it can also be used to predict both the reaction rate and the evolution of the Cu oxidation state during the steady-state experiments. The findings of this work are expected to have a positive contribution to a better mechanistic understanding of the MvK-type catalytic reactions in general.

2. Materials and methods

2.1. Materials

γ-Al_2O_3 was purchased from Sasol Germany (Puralox SCCA-30/170); the precursors of $CuCl_2{\cdot}2H_2O$ ($\geq$99%) and KCl ($\geq$99%) were purchased from Sigma-Aldrich.

All the gases, Ar (purity 5.0), He (purity 5.0), C_2H_4 (purity 3.5), O_2 (purity 5.0), HCl (20% in Ar, purity 3.5) were supplied by AGA.

2.2. Catalyst preparation and characterization

The catalysts were prepared by the incipient wetness impregnation method. The precursors ($CuCl_2{\cdot}2H_2O$ and KCl) were co-impregnated on the γ-Al_2O_3 with the calculated percentages, 5 wt% Cu, and 1.54 wt% K. After impregnation, the samples were put into the oven at 298 K for 10 h, after that, the samples were heated to 393 K with the ramping rate of 2 K/min and kept for 6 h. The obtained catalysts were sieved into 45–100 μm before catalytic tests. 5 wt% Cu loading was found to yield the optimal performance in terms of both the reaction rate constant and the yield of EDC, which was then selected in the present study. Besides, a volcano curve was also reported for the promotion effect of K, a moderate K loading of 1.54% was chosen here [5].

The specific surface area, pore volume, and pore size of the catalysts were measured on a TriStar 3020 instrument at 77 K using N_2 adsorption isotherms and BET, BJH analysis methods. Samples were degassed under vacuum at 473 K overnight before measurement.

XRD profiles were collected on a Bruker D8 Advanced DaVinci using the Cu Kα1 (0.154 nm wavelength).

Inductively coupled plasma optical-emission spectrometry (ICP-OES) was conducted on ThermoFisher Element 2 HR-ICP-MS. The solids were dissolved in a mixture of HNO_3/HCl (v/v = 1:3) until no solids were visible.

2.3. Transient experiments: Individual reduction and oxidation

The experiments were performed on the home-made operando fixed bed reactors (with the cross-section size of 5 mm × 10 mm) combined with MS (Omnistar GSD 3010: Pfeiffer Vacuum, Germany) and UV–vis-NIR spectroscopy (Avalight-DHS, Avantes) with a scanning circular area with a radius of 1 mm from the top of the catalyst bed at the gas inlet direction. The spatial distribution of $CuCl_2$ was measured by scanning along the catalyst bed where the reactor was moved in a controlled manner, while the probe kept fixed. More information about the setup can be obtained from our previous reports [32]. $CuCl_2$ concentration profile can be obtained from the d-d transition bands [25,32,34], in which no absorption can be observed for CuCl in the near-infrared

region. The $CuCl_2$ concentration can be quantified by the normalized Kubelka–Munk function with the obtained calibration curve.

Reactant gases were introduced into the reactor step-by-step with specified mass flow controllers. The catalyst was heated to the target reaction temperature in Ar with a ramping rate of 10 K/min, followed by activation with HCl to remove the paratacamite ($Cu_2(OH)_3Cl$) formed due to store in the atmosphere. The reduction and oxidation experiments were performed by introducing C_2H_4 and O_2 separately with the desired partial pressures with Ar served as the diluted gas and He as the tracer gas. The effluent gas was flowed to an online MS, with the UV–vis-NIR probing the top of the catalyst bed. Between the oxidation and reduction steps, Ar was flowed for at least 15 min to purge out the rest of C_2H_4 or O_2, which was left by the former step. Followed by flowing HCl for 4 min for the hydrochlorination step as the closure of the first cycle. The first and second cycles were used to fully activate the catalyst, the data got from the third cycle was used to perform the kinetic analysis. The method for calculating the reaction rate and removable Cl was reported in our previous reports [25,32]. Herein, the Gaussian multi-peak method was employed for deconvolution in the software of Origin.

2.4. Steady-state experiments

During the steady-state experiments, all the reactant gases, C_2H_4, O_2, and HCl were co-fed into the reactor with the required reactant gas molar ratio at the reaction temperature of 503 K. Two reaction conditions, with different reactant gas molar ratios and space velocities, were employed, one is stoichiometric (2:1:4), one is excess O_2 (1:2:2). The effluent gas stream was analyzed by MS and the UV–vis-NIR probe recording at the top of the catalyst bed. After reaching the steady-state, the probe of the UV–vis-NIR was moved along the catalyst bed to scan the catalyst for analysis of the $CuCl_2$ distribution.

The plug flow condition, pressure drop of the laboratory reactor, possible external and internal mass, and heat transport limitations at the reaction conditions were evaluated by a Eurokin fixed bed tool [44]. The results suggest that the kinetic studies at the conditions were not limited by external and internal limitations, and the pressure drop can be ignored. The details can be seen in the S1 of the Supporting information.

2.5. Reactor models

The laboratory fixed-bed quartz reactor is simulated by using a dynamic 1D pseudo-homogeneous model. There are two independent variables: z and t, the following assumptions have been incorporated in the development of the mathematical model (Table 1) [45],

(a) Temperature gradients between the catalyst bed and the fluid are small.
(b) Negligible changes of concentration and temperature gradients in the radial direction are assumed.
(c) The operation is isothermal.
(d) Diffusion along the axial direction is negligible compared to the convection.
(e) The average molecular mass of the reactants and products is constant along the axial direction.
(f) Pressure, density, and velocity of the gases in the system are assumed to be constant with time.

2.5.1. Initial and boundary conditions

The model equations can only be solved with appropriate initial and boundary conditions. The conditions for the dynamic model are listed below:

Initial conditions (t = 0):

Initially, it is assumed that the reactor is filled with a stagnant gas mixture with a given composition, pressure, and copper coordination (for all z)

$$\rho = \rho_0;\ u_s = u_{s,0};\ p = p_0;\ T = T_0;\ \omega_A = \omega_{A,0};\ C_{CuCl_2} = C_{CuCl_2,max} \quad (10)$$

Boundary conditions (t > 0):

$$\rho = \rho_0;\ u_s = u_{s,0};\ p = p_0;\ T = T_0;\ \omega_A = \omega_{A,0} \quad (11)$$

2.6. Temperature programmed reduction and oxidation

Ethylene temperature-programmed reduction (C_2H_4-TPR) was performed on the same fixed bed reactor and setup with MS recording the EDC signal. Before the TPR experiment, the catalyst was treated with two redox cycles as mentioned above to make sure the catalyst was fully oxidized to $CuCl_2$. Once a stable MS baseline was obtained at room temperature, the catalyst was reduced by 30% C_2H_4 in Ar with a flow rate of 120 ml/min, and at a ramping rate of 2 K/min to 503 K. The product EDC was recorded by an online MS, and the final temperature was kept until a stable MS signal was obtained.

Oxygen temperature-programmed oxidation (O_2-TPO) was performed after two redox cycles to make sure the $CuCl_2$ was fully reduced to CuCl. Afterward, the catalyst was exposed to 2% O_2 in Ar with a flow rate of 120 ml/min until a stable MS signal was obtained. Then the catalyst was heated to 503 K at a ramping rate of 10 K/min with the effluent gas stream recorded by an online MS. The O_2 consumption peak was obtained and used for analysis.

2.7. Derivation of reaction rate expressions from transient experiments

To well describe the experimental results, a kinetic model merging into a reactor model will be proposed and discussed. Herein, the kinetic model for ethylene oxychlorination is proposed based on transient experiments. In the oxychlorination process, EDC was produced in the reduction step as the product, as shown in Eq. (4), with $CuCl_2$ being reduced to CuCl. The catalyst was regenerated by the oxidation of CuCl to copper oxychloride (Cu_2OCl_2). We have reported that the third step of hydrochlorination was assumed to proceed too fast, hence it is kinetic irrelevant [25,32,33]. Thus, the reaction rate expressions are derived from the reduction and oxidation steps.

In the transient experiment, the ethylene reaction rate was measured as a function of time. The accumulative removed Cl from $CuCl_2$ was calculated from the consumed C_2H_4 based on the stoichiometric reaction of Eq. (4). It was found that the maximum Cl of 0.012 mol/g_{Cu} could be removed from $CuCl_2$ that was less than the theoretic value (0.016 mol/g_{Cu}). The Cl that can be removed from $CuCl_2$ by the ethylene reduction is

Table 1
Mass balance Equations.

Equation type	Equation	No.
Species mass fraction	$\frac{\partial \omega_A}{\partial t} = -\frac{1}{\rho\epsilon}\left(\epsilon\omega_A\frac{\partial \rho}{\partial t} + u_s\rho\frac{\partial \omega_A}{\partial z} + \rho\omega_A\frac{\partial u_s}{\partial z} + u_s\omega_A\frac{\partial \rho}{\partial z} - R_A{*}\rho{*}wt\%(1-\epsilon)\right)$	(7)
Momentum balance	$\frac{\partial P}{\partial Z} = -f\frac{\rho u_s^2}{d_p}$	(8)
Continuity	$\rho\frac{\partial u}{\partial Z} = 0$	(9)

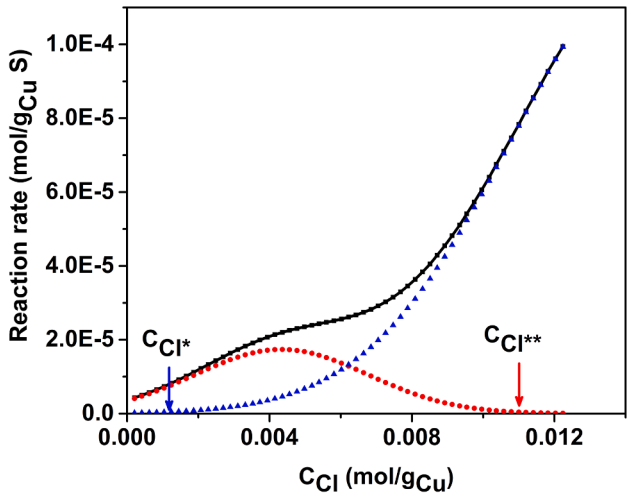

Fig. 1. The experimental reaction rate of reduction step vs Cl concentration of KCu/Al_2O_3. Blackline: experimental results; blue and red lines: deconvoluted rates contributed by Cu with 4- and 3-coordinated Cu, respectively. $C_{Cl^{**}}$ is the concentration at which the 3-coordinated Cu starts to form. $C_{Cl^{*}}$ is the concentration at which the 4-coordinated Cu was completely converted. Reaction conditions: T = 503 K, P_{tot} = 1 atm, $P_{C_2H_4}$ = 0.065 atm, W/F = 0.035 h·kg/mol. (For interpretation of the references to color in this figure legend, the reader is referred to the web version of this article.)

defined as removable Cl. The difference between the theoretical and measured maximum removable Cl is caused by the strong covalent bonding with alumina. The estimated reaction rates are shown in Fig. 1 as a function of removable Cl concentration on $CuCl_2/Al_2O_3$.

The experimental reaction rate curve (black line) can be deconvoluted into two parts using the Gaussian multiple peaks fit, as shown in Fig. 1. It suggests two types of active sites are possibly contributing to the reaction. The requirement of the active sites during the ethylene reduction of $CuCl_2$ was studied by DFT calculation [35,46]. During the reduction process, $CuCl_2$ is reduced to CuCl with Cl removed from the catalyst by C_2H_4, and the coordination number (CN) of Cu (i.e. the number of Cl atoms bonded with Cu) changes from 4 to 2 [35]. The surface Cl is rather mobile and randomly redistributed on the surface. It forms another type of Cu species with a 3-coordinated Cl, namely Cu with one Cl vacancy. Also, it should be noticed that the $CuCl_2$ catalyst is highly dispersed, close to a monolayer [26,47], and the concentration gradients between the bulk and surface can be ignored. DFT study also revealed that C_2H_4 directly attracted two adjunct Cl atoms at the Cu with 4-coordinated Cl, while the Cl atom can only be extracted one by one to produce EDC on the lower CN Cu [35,46]. It has been proved that the CuCl (Cu with 2-coordinated Cl) was inactive in this ethylene oxychlorination [29,36]. The region of high Cl concentration in Fig. 1 corresponds to the beginning of the reaction when Cu is in its original chemical state as $CuCl_2$. The first part (I) indicated by the blue line in Fig. 1 is the rate contributed from the Cu with 4-coordinated Cl, where the Cl–Cl pair is the active site. The second part (II) indicated by the red line in Fig. 1 is the rate contributed from Cu with 3-coordinated Cl, where the Cu–Cl pair is the active site [35]. The diverse changing of the Cu coordination number of Cu also indicated the dynamic character of the active site.

Therefore, the rate expressions for the reduction step are divided into two parts.

$$r_1 = r_{1,I} + r_{1,II} \tag{12}$$

On Cu with 4-coordinated Cl (CN = 4), ethylene extracts two Cl atoms and forms EDC (Eq. (13)) as indicated by DFT calculation [46].

$$2CuCl_2{}^{*} + C_2H_4 \rightarrow 2CuCl + C_2H_4Cl_2{}^{*} \tag{13}$$

The reaction rate for the elementary step of Eq. (13) is described by Eq. (14):

$$r_{1,I} = k_{1,I} P_{C_2H_4} \left(C_{Cl} - C_{Cl}^{*}\right)^2 \tag{14}$$

where C_{Cl} is the removable Cl of $CuCl_2$, Cl* is the threshold of Cu with 4-coordinated completely consumed.

On $CuCl_2$ with Cl vacancy where the surface has a relatively low Cu coordination number with Cl (CN = 3), DFT calculation suggested that ethylene binds with the Cu atom and then is chlorinated one by one to form EDC [35,46], as shown in Eqs. (15)–(17):

$$C_2H_4 + {}^{*} \rightleftharpoons C_2H_4{}^{*} \tag{15}$$

$$\square - CuCl_2 + C_2H_4{}^{*} \rightarrow CuCl + C_2H_4Cl^{*} \tag{16}$$

$$\square - CuCl_2 + C_2H_4Cl^{*} \rightarrow CuCl + C_2H_4Cl_2 \tag{17}$$

where * is the active site of the Cu-Cl pair. $\square - CuCl_2$ represents $CuCl_2$ with vacancy. Step (16) is assumed to be the rate-determining step based on the DFT study [35,46], and the rate expression is

$$r_{1,II} = k_{1,II} P_{C_2H_4} (C_{Cl}^{**} - C_{Cl}) C_{Cl} \tag{18}$$

where C_{Cl}^{**} is the threshold that Cu with 3-coordinated Cl, $C_{Cl}^{**} - C_{Cl}$ corresponding to the vacancy concentration, and first-order is to Cl and the vacancy.

When Cl concentration is higher than C_{Cl}^{**}, the reaction rate representing the second active site ($r_{1,II}$) is zero, while the Cl concentration is lower than C_{Cl}*, the reaction rate representing the first active site ($r_{1,I}$) is zero.

The reduction ends with all the reducible $CuCl_2$ was reduced to CuCl. As shown in Eq. (5), in the oxidation step, CuCl was re-oxidized to Cu oxychloride (Cu_2OCl_2) [15,25,28,32]. The oxygen conversion was measured as a function of time. The accumulative insertion of O into CuCl was calculated from the consumed O_2-based on the stoichiometric reaction of Eq. (5). The oxidation reaction rate (black line) with the concentration of CuCl is plotted in Fig. 2. Similar to the reduction rate curve in Fig. 1, the rate curve was deconvoluted into two curves (red and

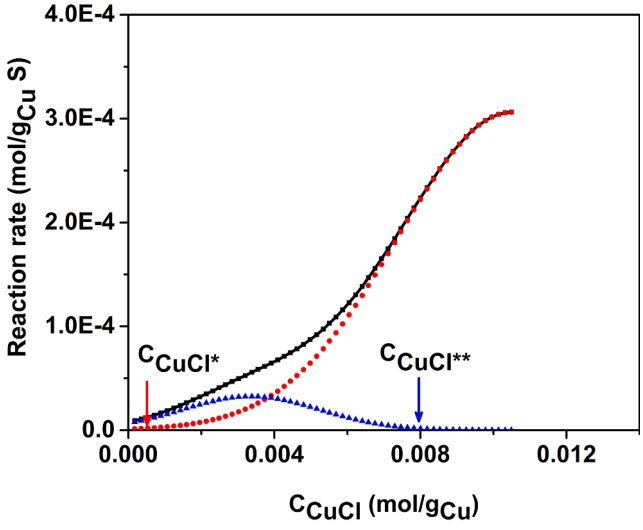

Fig. 2. The experimental reaction rate of oxidation step vs CuCl concentration of KCu/Al_2O_3. Blackline: experimental results; red and blue lines: deconvoluted results using the Gaussian multiple-peak fitting method. the point of $C_{CuCl^{*}}$ represents 2-coordinated Cu does not exist; $C_{CuCl^{**}}$ represents the starting point where 2- and 3-coordinated Cu occurs. Reaction conditions: T = 503 K, P_{tot} = 1 atm, P_{O_2} = 0.3 atm, W/F = 0.02 h·kg/mol. (For interpretation of the references to color in this figure legend, the reader is referred to the web version of this article.)

blue lines). The oxidation rate of CuCl can also be described by the summary of the two contributions:

$$r_2 = r_{2,I} + r_{2,II} \tag{19}$$

At the beginning of the reaction, Cu is in the form of CuCl with the coordination number of 2. Based on the DFT calculations [35,46], the elementary reaction steps involve oxygen adsorption, dissociation, and the reconstructing are presented in steps (Eqs. (20)–(22)). The oxidation requires the Cu–Cl vacancy pair as the active site. The oxygen adsorbed on Cu sites and reacts with two adjunct CuCl to form Cu_2OCl_2, while the coordination number becomes 4.

$$O_2 + * \underset{k_{-2A}}{\overset{k_{2A}}{\rightleftarrows}} O_2* \tag{20}$$

$$O_2* + 2CuCl \underset{k_{-2B}}{\overset{k_{2B}}{\rightleftarrows}} 2CuOCl + * \tag{21}$$

$$CuOCl + CuCl \underset{k_{-2C}}{\overset{k_{2C}}{\rightleftarrows}} Cu_2OCl_2 \tag{22}$$

Herein, the surface reaction (Eq. (21)) is usually the rate-determine step, therefore the rate expression becomes:

$$r_2 = k_{2B}\theta_{O_2} C_{CuCl}^2 \tag{23}$$

Moreover, the number of active sites is a conserved quantity:

$$\theta_{O_2} + \theta_* = 1 \tag{24}$$

For simplicity, in the final rate equation, the rate constant k_{2B} will be referred to as k_2 and the adsorption equilibrium constant for O_2, K_{2A}, will be referred to as K_{eq}. The reaction rate of the oxidation step becomes:

$$r_{2,I} = \frac{k_{2,I} P_{O_2} (C_{CuCl} - C_{CuCl}^*)^2}{1 + P_{O_2} K_{eq}} \tag{25}$$

With the progress of the oxidation, the adjunct two CuCl moieties are not available, the elementary reaction step changes to:

$$O_2* + CuCl \underset{k_{-2B,II}}{\overset{k_{2B,II}}{\rightleftharpoons}} O* + CuOCl + * \tag{26}$$

The rate expression is described by Eq. (27):

$$r_{2,II} = \frac{k_{2,II} P_{O_2} (C_{CuCl}^{**} - C_{CuCl}) C_{CuCl}}{1 + P_{O_2} K_{eq}} \tag{27}$$

where the first-order is to the intermediate CuCl and expressed by $(C_{CuCl}^{**} - C_{CuCl})C_{CuCl}$.

3. Results and discussion

3.1. Catalyst texture properties

The physical properties like surface area, pore volume, and pore size of the fresh catalysts are summarized in Table 2. The Cu and K loadings were verified by ICP-OES, as shown in Table 2. Adding promoter to the catalyst, the surface area, pore volume, and pore size slightly decreased compared with the neat $CuCl_2/Al_2O_3$ catalyst. Fig. 3 shows the XRD patterns for the fresh neat $CuCl_2/Al_2O_3$ and K-promoted catalysts. No obvious diffraction peaks for $CuCl_2$ and KCl can be observed, indicating that $CuCl_2$ on the Al_2O_3 support is well dispersed. It was reported that $CuCl_2$ is highly dispersed on the alumina surface with different techniques, like chemisorption, and EXAFS, etc. [25,29,47,48]. When the neat Cu catalyst was doped with K, no obvious difference was displayed on the XRD patterns [33]. But at $2\theta \sim 15°$, for the neat Cu catalyst, there is a peak assigned to the paratacamite ($Cu_2(OH)_3Cl$), which was produced due to the catalyst being stored in the air [25,32]. However, no traces of paratacamite was found on the K-promoted catalyst, which is confirmed with the previous reports [25,30]. No differences in the XRD patterns were observed on the spent catalysts compared to the fresh ones.

Table 2
Physical properties and elements analysis of the catalysts.

Catalyst	Surface area (m^2/g)	Pore volume (cm^3/g)	Pore size (Å)	Cu (wt %)	K (wt %)
Cu/Al_2O_3	137	0.39	81.7	5.1	–
KCu/Al_2O_3	129	0.37	81.0	5.0	1.3

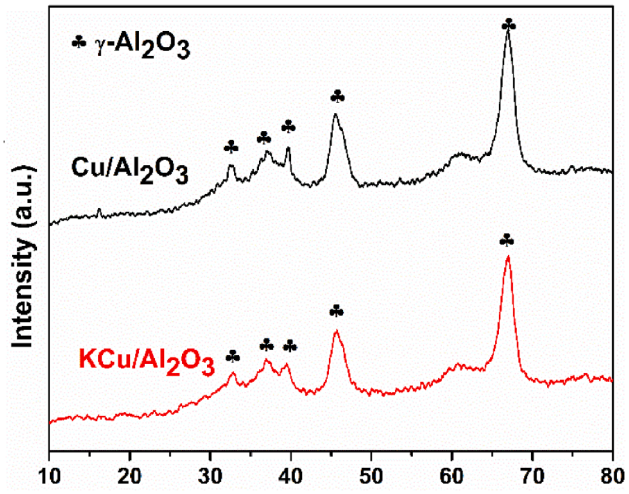

Fig. 3. XRD patterns of Cu/Al_2O_3, KCu/Al_2O_3.

3.2. Verification of the kinetic model

The kinetic parameters ($k_{1,I}$, $k_{1,II}$, $k_{2,I}$, $k_{2,II}$,) were estimated at each temperature by the non-linear model regression (see the Supporting information S5). All the *F*-value for the global significance of the regression were found to be considerably larger than the tabulated one, i.e., 3.27. The statistical significance of each parameter estimate is also assessed by a *T*-test. The individual confidence intervals of the estimated parameters were calculated at a 95% probability.

The kinetic models are then validated by the comparison between model-simulated and experimental values. The comparison between the simulated removable Cl in the reduction step and CuCl in the oxidation step based on the kinetic models with the experimental values at different temperatures is presented in Fig. 4. As the reduction proceeds, $CuCl_2$ is reduced to CuCl, Cl is removed from the catalyst by C_2H_4 with the forming of EDC as the product. The simulation and experimental curves of C_{Cl} with time on stream fit quite well as shown in Fig. 4a of the reduction step. As is expected, the higher temperature, the higher the reaction rate. In the oxidation step, CuCl was oxidized to copper oxychloride by O_2, with no gas-phase product formed. The CuCl concentration with time on stream was shown in Fig. 4b, the simulation, and experimental results are also well fitted. It is noted that the experimental Cl or CuCl concentration is calculated by using the mass balances from the reaction, and simulated Cl concentration is calculated using the differential reactor model.

$$-\frac{dC_{Cl}}{dt} = r_1 \quad t = 0: \; C_{Cl} = C_{Cl,\,0} \tag{28}$$

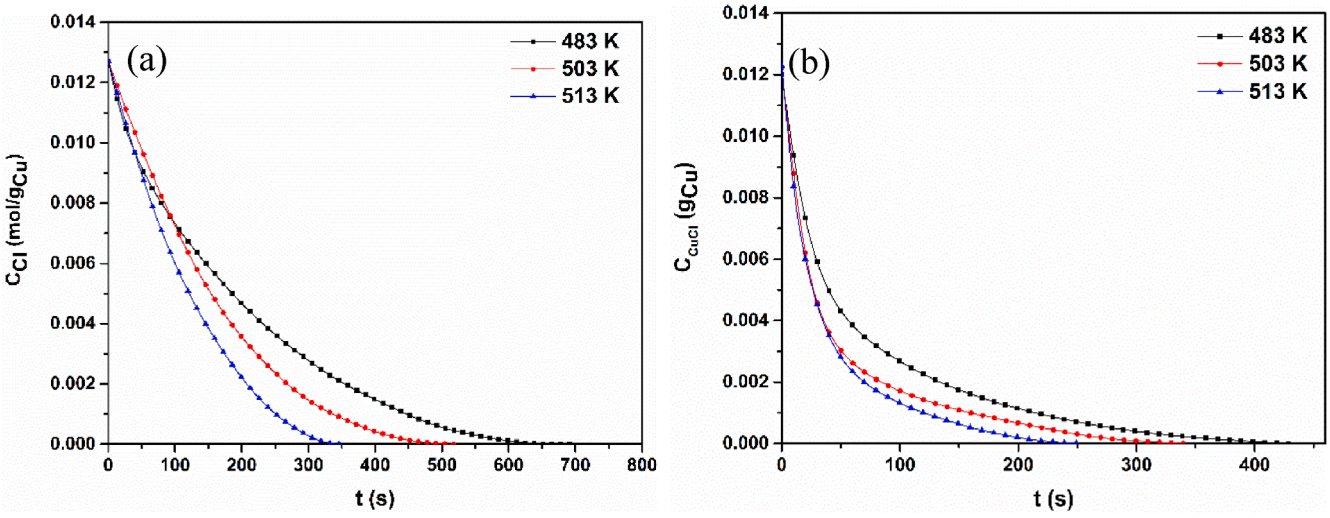

Fig. 4. The simulated Cl and CuCl concentration obtained from integration of the two-part rate expressions (line) and experimental (symbol) reaction for the KCu/Al_2O_3 catalyst (a) reduction; (b) oxidation. Reaction conditions: $P_{C_2H_4}$ = 0.065 atm or P_{O_2} = 0.3 atm, P_{tot} = 1 atm.

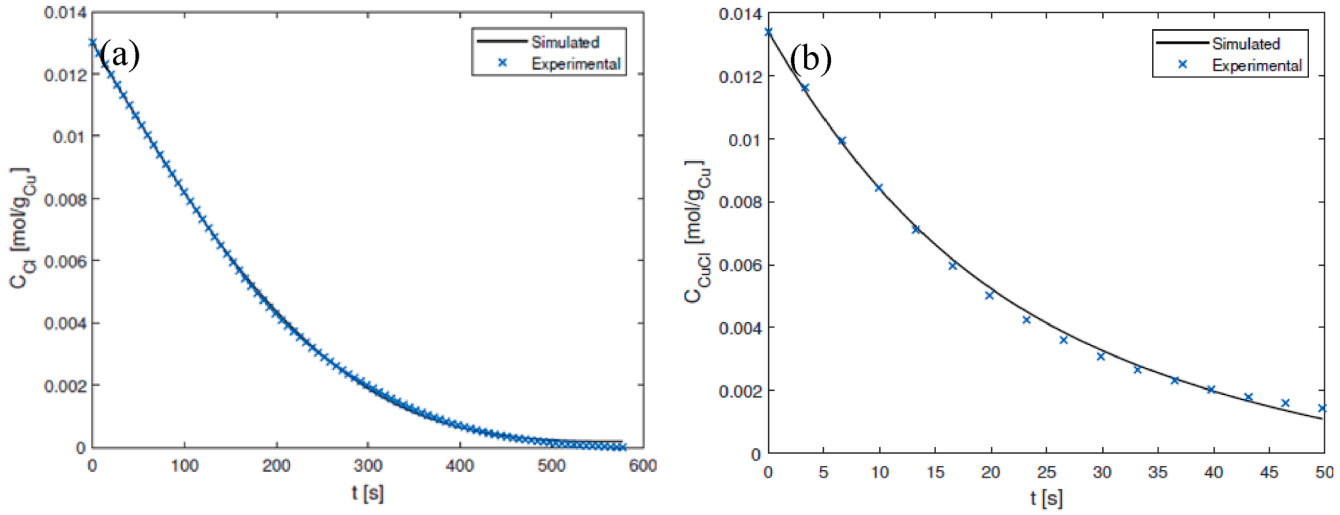

Fig. 5. The simulated (line) Cl and CuCl concentration obtained from integration of the two-part rate expressions, and experimental (symbol) reaction for the KCu/Al_2O_3 catalyst (a) reduction; (b) oxidation. Reaction conditions: $P_{C_2H_4}$ = 0.1 atm or P_{O_2} = 0.1 atm, T = 503 K, P_{tot} = 1 atm.

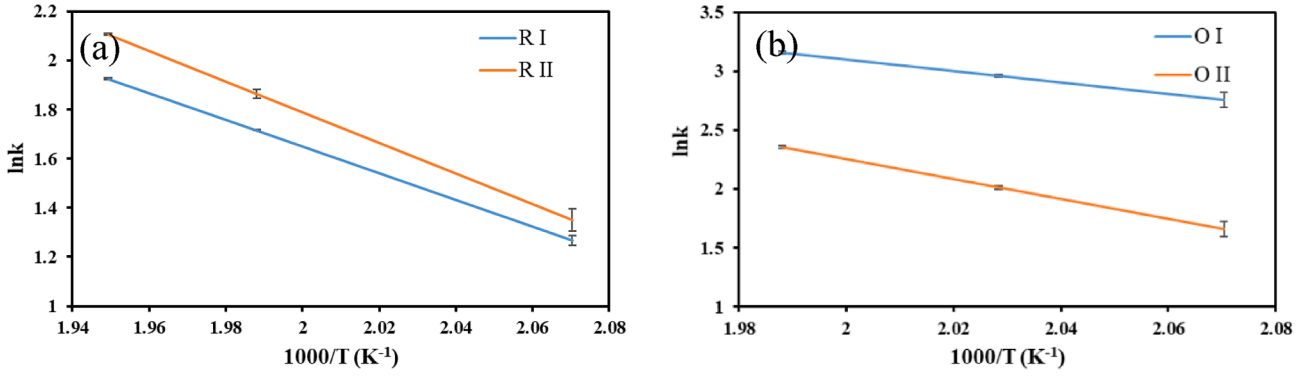

Fig. 6. Arrhenius plot for reduction and oxidation steps for KCu/Al_2O_3 catalyst. Part I and part II of the two-part rate expression for the a) reduction, and b) oxidation steps. The error bars represent the 95% confidence interval of the estimated k.

Table 3
Estimated pre-exponential factors (A) and activation energies (E_a) for the respective reduction and oxidation half cycles for the KCu/Al_2O_3 catalyst, with 95% confidence intervals and correlation coefficients of R^2, and the threshold concentrations in Figs. 1 and 2.

Parameter	Unit	Reduction	Oxidation
K_{eq}	atm^{-1}	–	0.2
A_I	$g_{Cu}\ mol^{-1}\ atm^{-1}\ s^{-1}$	$2.78 \times 10^5 \pm 4.90 \times 10^3$	$3.64 \times 10^5 \pm 2.00 \times 10^4$
A_{II}	$g_{Cu}\ mol^{-1}\ atm^{-1}\ s^{-1}$	$1.58 \times 10^6 \pm 5.00 \times 10^3$	$2.00 \times 10^8 \pm 3.00 \times 10^6$
$E_{a,\ I}$	$kJ\ mol^{-1}$	45.25 ± 0.48	40.35 ± 0.42
$E_{a,\ II}$	$kJ\ mol^{-1}$	51.90 ± 0.41	70.10 ± 0.65
R^2_I	–	0.992	0.996
R^2_{II}	–	0.998	1.000
$C_{Cl^{**}}$	mol/g_{Cu}	0.002	–
$C_{Cl^{*}}$	mol/g_{Cu}	0.012	–
$C_{CuCl^{**}}$	mol/g_{Cu}	–	0.002
$C_{CuCl^{*}}$	mol/g_{Cu}	–	0.008

$$-\frac{dC_{CuCl}}{dt} = r_2 \quad t = 0: \ C_{CuCl} = C_{CuCl,\ 0} \tag{29}$$

The kinetic models are further validated at another partial pressure, as shown in Fig. 5. For both reduction and oxidation processes, the simulation and experimental results fit quite well, suggesting that the kinetic models describe well the concentration dependence of ethylene and oxygen. So far, we have demonstrated for the K-promoted catalyst, the kinetic model can fit well with the experimental results at different temperatures and partial pressures. We can use this model to study and analyze the reduction-oxidation cycle.

The dynamic change of $CuCl_2$ concentration can be derived from the rate expressions. Firstly, the Cl concentration is equivalent to the reducible $CuCl_2$ concentration:

$$C_{Cl} = C_{CuCl_2} \tag{30}$$

Secondly, the total Cu concentration is conserved,

$$C_{CuCl} = C_{CuCl_2,0} - C_{CuCl_2} \tag{31}$$

By inserting the rate expressions of reduction and oxidation, the rate of disappearance of $CuCl_2$ is

$$\frac{dC_{CuCl_2}}{dt} = r_2 - r_1 = \begin{bmatrix} k_{2,I}P_{O_2}\left(C_{CuCl_2,0} - C_{CuCl_2} - CuCl^{*}\right)^2 \\ +k_{2,II}P_{O_2}\left(CuCl^{**} - C_{CuCl_2,0} + C_{CuCl_2}\right)\left(C_{CuCl_2,0} - C_{CuCl_2}\right) \\ -k_{1,I}P_{C_2H_4}\left(C_{CuCl_2} - Cl^{*}\right)^2 - k_{1,II}P_{C_2H_4}\left(Cl^{**} - C_{CuCl_2}\right)C_{CuCl_2} \end{bmatrix} \Big/ \left(1 + K_{eq}P_{O_2}\right) \tag{32}$$

The parameter fitting was done firstly at constant temperatures to obtain the rate constants of k values based on the data of Fig. 4. The $k_{1,I}$, $k_{1,II}$, $k_{2,I}$, $k_{2,II}$ values with the 95% confidence intervals as error bars are presented in Fig. 6, which follow well the Arrhenius plots. The activation energies, E_a, and pre-exponential factors are summarized in Table 3.

Both the reduction and oxidation steps $E_{a,\ II}$ is larger than $E_{a,\ I}$. For the reduction, the energy barrier is higher on the $CuCl_2$ with the Cl vacancy than the $CuCl_2$ without the Cl vacancy. For the oxidation step, the energy barrier is also higher on CuOCl with O vacancy than that on the neat CuCl. The pre-exponential factors (A) for the oxidation step are bigger than the ones of the reduction step. The rate constants for the oxidation steps are much higher than that in the reduction step. A similar conclusion that the oxidation step was more favorable than the reduction step can also be obtained from the C_2H_4-TPR and O_2-TPO (shown in Fig. S1), the peak positions shifted to a lower one on the TPO compared to the TPR.

3.3. Simulation and kinetic modeling of the steady-state experiments

Based on the above discussion, it has been proved that the developed kinetic model can correctly describe the transient behavior of the reduction and oxidation for the K-promoted $CuCl_2/Al_2O_3$ catalyst. In our previous reports, we utilized the home-made operando setups combined UV–vis-NIR and MS to study the kinetics and catalyst composition changes in the redox process [25,32–34]. Using our developed methodology, the $CuCl_2$ profiles and C_2H_4 reaction rate (or conversion) can be monitored simultaneously during the steady-state experiment where C_2H_4, O_2, and HCl are co-fed together.

Since the active sites of the catalyst are highly dynamic, it is necessary to calculate the rate of change of $CuCl_2$ concentration with time.

The laboratory reactor is simulated using Eqs. (7)–(9), and the related parameters are listed in Table S1. The consumption ethylene rate of R_A in Eq. (7) is the rate of the ethylene oxychlorination.

The simulation is performed without any change in kinetic parameters in Table 3 obtained from the transient kinetic modeling. Furthermore, the dynamic evolution of $CuCl_2$ concentration (Eq. (32)) is also solved together with reactor simulation. The transient kinetic model can be simplified to the steady-state kinetic model, at the steady-state:

$$\frac{dC_{CuCl_2}}{dt} = 0 \tag{33}$$

$$r_1 = r_2 \tag{34}$$

The evolution of ethylene conversion and the $CuCl_2$ concentration of the simulated and experimental $CuCl_2$ profiles during the steady-state is shown in Fig. 7. From Fig. 7a and the previous reports [25,32,33], we have demonstrated that the reaction was in the region of high $CuCl_2$ (or Cl) concentration at the steady-state. As we discussed above, at a high concentration of Cl, the rate representing the first active site, $r_{1,I}$ is dominating, hence, the total reaction rate can be approximately expressed by $r_{1,I}$. At a low concentration of CuCl, the rate representing the second active site, $r_{2,II}$ is dominating, and the oxidation rate can be approximated by $r_{2,II}$. Eq. (34) becomes:

$$r_{1,I} = r_{2,II} \tag{35}$$

To get the steady-state expression, it was assumed that the C^{**}_{CuCl} may be approximated by the maximum concentration of CuCl at the steady-state. Also, it was assumed that the C^{*}_{Cl} was negligible at steady-state.

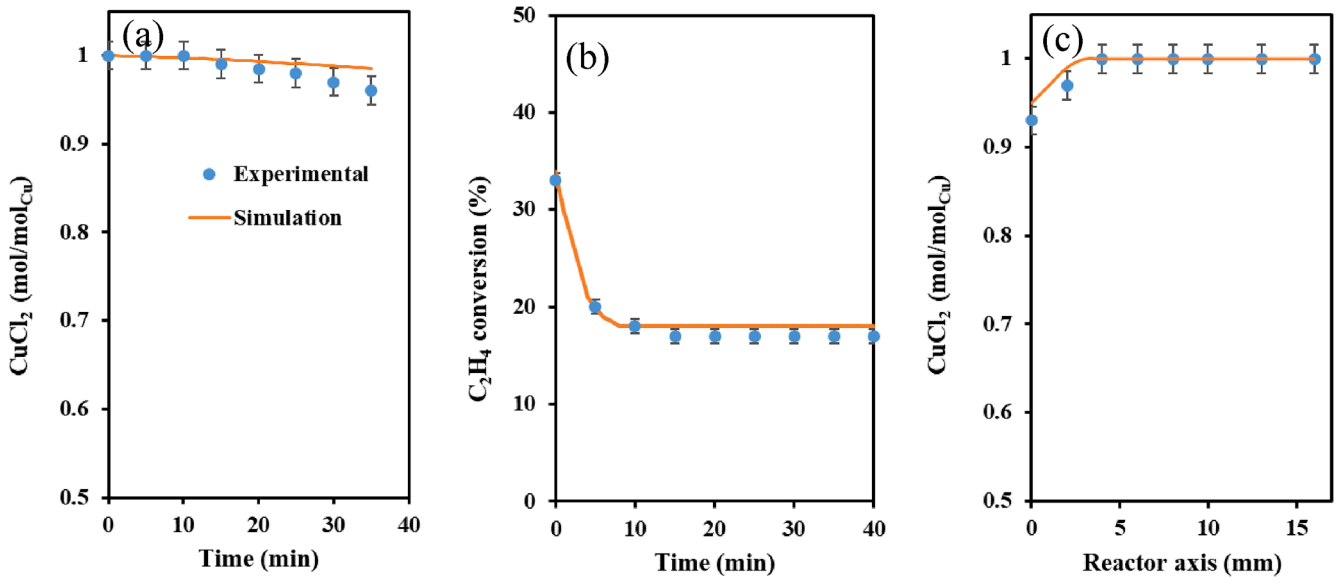

Fig. 7. The simulated and experimental results in the steady-state. (a) Total $CuCl_2$ concentration at the top of catalyst bed with time on stream, (b) C_2H_4 conversion with time on stream, (c) total $CuCl_2$ concentration vs reactor axis in the steady-state. Reaction condition: $W_{cat} = 0.7$ g, T = 503 K, $P_{tot} = 1$ atm, $P_{C_2H_4} = 0.009$atm, $W/F_{eth,0} = 0.19$ h kg mol^{-1}, gas molar ratio: $C_2H_4/O_2/HCl = 2/1/4$. The error bars represent the standard deviation mean of three experimental replicates, the $CuCl_2$ is calculated using the calibration curve, and the error bar is estimated for the calibration curve [32].

Table 4
Comparison of the experimental reaction rate and $CuCl_2$ concentration, and the simulated ones. (the detailed reaction conditions can be found in Figs. 7 and S2).

Condition	Parameter	Reaction rate (mol/(g s))	$CuCl_2$ (mol/mol_{Cu})
I (2:1:4)	Simulated	2.63×10^7	0.98
	Experimental	2.49×10^7	0.96
II (1:2:2)	Simulated	1.50×10^6	0.79
	Experimental	1.44×10^6	0.79

The CuCl can be expressed as:

$$C_{CuCl} = C_{CuCl,max} - C_{Cl} \tag{36}$$

It is noted that in the steady-state, the O_2 adsorption term $(1 + K_{eq}P_{O_2})$ should also be included in the reduction process. The Cl concentration in $CuCl_2$ and the rate expression at the steady-state are described as Eqs. (37) and (38), respectively, (the detailed derivation of the equations can be seen in S3 Supporting information):

$$C_{Cl} = \frac{C_{CuCl,max}}{1 + \frac{k_{1,I}P_{C_2H_4}}{k_{2,II}P_{O_2}}} \tag{37}$$

$$r_{steady-state} = \frac{k_{1,I}\left(C_{CuCl,max}\right)^2 P_{C_2H_4}P_{O_2}^2}{\left(P_{O_2} + \frac{k_{1,I}}{k_{2,II}}P_{C_2H_4}\right)^2\left(1 + K_{eq}P_{O_2}\right)} \tag{38}$$

We have reported that the gradual decrease of C_2H_4 conversion in the initial period was attributed to the dynamic process to achieve the steady-state [25]. The results indicated the kinetic model fitted well with the experimental results. It shows that over half of the reducible Cu is in the oxidized chemical state. It is greatly increased compared to the unpromoted Cu catalyst, in which we have reported that roughly 0.4 mol Cu was kept oxidized of $CuCl_2$ [32]. It indicates the positive effect of K as a promoter in the regenerating of $CuCl_2$ in ethylene oxychlorination. Besides, the dynamic changes of the $CuCl_2$ were studied at the different positions along the reactor by moving the UV–vis-NIR probe during the steady-state, gaining a better understanding of the kinetic model, as shown in Fig. 7c. It is evident that K promotion favors the $CuCl_2$ oxidation state, which dominates along the catalyst bed, thus the catalysts are stable. Table 4 shows C_2H_4 reaction rate and $CuCl_2$ concentration at the steady-state for both simulated and experimental data, which matched very well with less than 5% deviation. The simulation was also performed for different feeding conditions (1:2:2, excess O_2), shown in Fig. S2 of SI, the experimental and simulated C_2H_4 reaction rate and $CuCl_2$ concentration can also fitted well.

In ethylene oxychlorination, both the solid phase and gas phase are likely mobile on the catalyst surface. Especially for the co-feeding steady-state, it will create a more complicated surface environment than the transient reduction and oxidation reactions separately. All the above results of the simulation and experimental fit well, showing the accuracy of the kinetic model. This model can be used to predict and analyze the reaction rate and Cu oxidation state during the steady-state experiments.

4. Conclusions

Kinetic study of ethylene oxychlorination, a vital process involved in VCM production, was performed at 483–513 K, atmospheric pressure on the K-doped $CuCl_2/\gamma$-Al_2O_3 catalyst. A new approach for kinetic modeling of the MvK-type process was developed taking into account the dynamic changing characters of the active sites in the redox cycle. The new approach includes detailed kinetic modeling at three levels, including the transient kinetic model for half-reactions in the redox cycle of reduction of $CuCl_2$ by C_2H_4 and oxidation of CuCl by O_2, a transient kinetic model of the whole redox cycle by combining the kinetic models of the half-reactions, and the steady-state reaction, to study and evaluate the reaction kinetics. A kinetic model describing the transient and steady-state behaviors combining the reactant gas-phase and catalyst solid-phase in the reaction including the reaction rate and Cu oxidation state has been developed with the best fitting. The transient reaction rates fit the corresponding experimental results for a variety of temperatures and partial pressures. The simulated steady-state reaction rate is also in good agreement with the analogous experimental reaction rates. Furthermore, the simulated evolution of $CuCl_2$ concentration during the steady-state is also fittingly matched with the experimental result. This kinetic model can accurately predict the gas- and solid-phase catalytic behaviors during the steady-state without doing any complicated computation. This model can be used to predict the conversion and spatial-time $CuCl_2$ concentration decently well, which are the two most important factors for this

industrial process. It hence has been implied that applying the transient experiments to extract the correlated kinetic parameters for building the model to further describe the steady-state is a reliable and efficient method to study the kinetics of the MvK-type of catalytic reactions. Therefore, the industrial application of this kinetic model can be expected as it is easy to perform. It is also expected that this method can be exploited to other catalytic reaction systems, in which redox cycles are involved, especially for MvK-type reactions in general.

Declaration of Competing Interest

The authors declare that they have no known competing financial interests or personal relationships that could have appeared to influence the work reported in this paper.

Acknowledgements

We gratefully acknowledge the financial support from iCSI (industrial Catalysis Science and Innovation), a center for Researched-based Innovation funded by the Research Council of Norway under grant No. 237922.

Appendix A. Supplementary data

Supplementary data to this article can be found online at https://doi.org/10.1016/j.cej.2020.128013.

References

[1] P. Mars, D.W. van Krevelen, Oxidations carried out by means of vanadium oxide catalysts, Chem. Eng. Sci. 3 (1954) 41–59.
[2] P. Arpentinier, F. Cavani, F. Trifirò, The technology of catalytic oxidations, Technip Paris (2001).
[3] V.H. Vu, J. Belkouch, A. Ould-Dris, B. Taouk, Catalytic oxidation of volatile organic compounds on manganese and copper oxides supported on titania, AIChE J. 54 (2008) 1585–1591.
[4] Z.G. Lei, B. Han, K. Yang, B.H. Chen, Influence of H_2O on the low-temperature NH_3-SCR of NO over V_2O_5/AC catalyst: an experimental and modeling study, Chem. Eng. J. 215 (2013) 651–657.
[5] H. Ma, Y. Wang, Y. Qi, K.R. Rout, D. Chen, Critical review of catalysis for ethylene oxychlorination, ACS Catal. 10 (2020) 9299–9319.
[6] A. Beretta, A. Lanza, L. Lietti, S.A. Clave, J. Collier, M. Nash, An investigation on the redox kinetics of NH_3-SCR over a V/Mo/Ti catalyst: evidence of a direct role of NO in the re-oxidation step, Chem. Eng. J. 359 (2019) 88–98.
[7] M.A. Vannice, An analysis of the Mars–van Krevelen rate expression, Catal. Today 123 (2007) 18–22.
[8] C. Doornkamp, V. Ponec, The universal character of the Mars and van Krevelen mechanism, J. Mol. Catal. A: Chem. 162 (2000) 19–32.
[9] K. Routray, G. Deo, Kinetic parameter estimation for a multiresponse nonlinear reaction model, AIChE J. 51 (2005) 1733–1746.
[10] T. Malleswara Rao, G. Deo, Kinetic parameter analysis for propane ODH: V_2O_5/Al_2O_3 and MoO_3/Al_2O_3 catalysts, AIChE J. 53 (2007) 1538–1549.
[11] H. Chen, Y. Yan, Y. Shao, H. Zhang, H. Chen, Catalytic combustion kinetics of isopropanol over novel porous microfibrous-structured ZSM-5 coating/PSSF catalyst, AIChE J. 61 (2015) 620–630.
[12] D. Widmann, R.J. Behm, Dynamic surface composition in a Mars–van Krevelen type reaction: CO oxidation on Au/TiO_2, J. Catal. 357 (2018) 263–273.
[13] E.J. Grootendorst, Y. Verbeek, V. Ponec, The role of the Mars and Van Krevelen mechanism in the selective oxidation of nitrosobenzene and the deoxygenation of nitrobenzene on oxidic catalysts, J. Catal. 157 (1995) 706–712.
[14] E. Finocchio, N. Rossi, G. Busca, M. Padovan, G. Leofanti, B. Cremaschi, A. Marsella, D. Carmello, Characterization and catalytic activity of $CuCl_2$-Al_2O_3 ethylene oxychlorination catalysts, J. Catal. 179 (1998) 606–618.
[15] C. Lamberti, C. Prestipino, F. Bonino, L. Capello, S. Bordiga, G. Spoto, A. Zecchina, S. Diaz Moreno, B. Cremaschi, M. Garilli, A. Marsella, D. Carmello, S. Vidotto, G. Leofanti, The chemistry of the oxychlorination catalyst: an in situ, time-resolved XANES study, Angew. Chem. Int. Ed. 41 (2002) 2341–2344.
[16] K.S. Go, Y. Kim, S. Real Son, S.D. Kim, 1,2-Dichloroethane production by two-step oxychlorination reactions in a fluidized bed reactor, Chem. Eng. Sci. 65 (2010) 499–503.
[17] P. Kappen, J.-D. Grunwaldt, B.S. Hammershøi, L. Tröger, B.S. Clausen, The state of Cu promoter atoms in high-temperature shift catalysts—an in situ fluorescence XAFS study, J. Catal. 198 (2001) 56–65.
[18] M.R. Flid, Vinyl chloride technology: present and future, Catal. Ind. 1 (2009) 285–293.
[19] Z. Vajglová, N. Kumar, K. Eränen, A. Tokarev, M. Peurla, J. Peltonen, D.Y. Murzin, T. Salmi, Influence of the support of copper catalysts on activity and 1,2-dichloroethane selectivity in ethylene oxychlorination, Appl. Catal. A: Gen. 556 (2018) 41–51.
[20] D. Shi, R. Hu, Q. Zhou, L. Yang, Catalytic activities of supported perovskite promoter catalysts La_2NiMnO_6–$CuCl_2$/γ-Al_2O_3 and $La_{1.7}K_{0.3}NiMnO_6$–$CuCl_2$/γ-Al_2O_3 for ethane oxychlorination, Chem. Eng. J. 288 (2016) 588–595.
[21] R. Lin, A.P. Amrute, J. Pérez-Ramírez, Halogen-mediated conversion of hydrocarbons to commodities, Chem. Rev. 117 (2017) 4182–4247.
[22] H. Ma, G. Ma, Y. Qi, Y. Wang, Q. Chen, K.R. Rout, T. Fuglerud, D. Chen, Nitrogen-doped carbon-assisted one-pot tandem reaction for vinyl chloride production via ethylene oxychlorination, Angew. Chem. Int. Ed. 59 (2020) 22080–22085.
[23] C. Lamberti, C. Prestipino, L. Capello, S. Bordiga, A. Zecchina, G. Spoto, S. Moreno, A. Marsella, B. Cremaschi, M. Garilli, The $CuCl_2$/Al_2O_3 catalyst investigated in interaction with reagents, Int. J. Mol. Sci. 2 (2001) 230–245.
[24] N.B. Muddada, U. Olsbye, L. Caccialupi, F. Cavani, G. Leofanti, D. Gianolio, S. Bordiga, C. Lamberti, Influence of additives in defining the active phase of the ethylene oxychlorination catalyst, Phys. Chem. Chem. Phys. 12 (2010) 5605.
[25] K.R. Rout, E. Fenes, M.F. Baidoo, R. Abdollahi, T. Fuglerud, D. Chen, Highly active and stable CeO_2-promoted $CuCl_2$/Al_2O_3 oxychlorination catalysts developed by rational design using a rate diagram of the catalytic cycle, ACS Catal. 6 (2016) 7030–7039.
[26] G. Leofanti, M. Padovan, M. Garilli, D. Carmello, A. Zecchina, G. Spoto, S. Bordiga, G.T. Palomino, C. Lamberti, Alumina-supported copper chloride, J. Catal. 189 (2000) 91–104.
[27] G. Leofanti, A. Marsella, B. Cremaschi, M. Garilli, A. Zecchina, G. Spoto, S. Bordiga, P. Fisicaro, G. Berlier, C. Prestipino, G. Casali, C. Lamberti, Alumina-supported copper chloride, J. Catal. 202 (2001) 279–295.
[28] G. Leofanti, A. Marsella, B. Cremaschi, M. Garilli, A. Zecchina, G. Spoto, S. Bordiga, P. Fisicaro, C. Prestipino, F. Villain, C. Lamberti, Alumina-supported copper chloride, J. Catal. 205 (2002) 375–381.
[29] N.B. Muddada, U. Olsbye, G. Leofanti, D. Gianolio, F. Bonino, S. Bordiga, T. Fuglerud, S. Vidotto, A. Marsella, C. Lamberti, Quantification of copper phases, their reducibility and dispersion in doped-$CuCl_2$/Al_2O_3 catalysts for ethylene oxychlorination, Dalton Trans. 39 (2010) 8437–8449.
[30] N.B. Muddada, U. Olsbye, T. Fuglerud, S. Vidotto, A. Marsella, S. Bordiga, D. Gianolio, G. Leofanti, C. Lamberti, The role of chlorine and additives on the density and strength of Lewis and Brønsted acidic sites of γ-Al_2O_3 support used in oxychlorination catalysis: a FTIR study, J. Catal. 284 (2011) 236–246.
[31] D. Gianolio, N.B. Muddada, U. Olsbye, C. Lamberti, Doped-$CuCl_2$/Al_2O_3 catalysts for ethylene oxychlorination: influence of additives on the nature of active phase and reducibility, Nucl. Instrum. Methods Phys. Res. B 284 (2012) 53–57.
[32] K.R. Rout, M.F. Baidoo, E. Fenes, J. Zhu, T. Fuglerud, D. Chen, Understanding of potassium promoter effects on oxychlorination of ethylene by operando spatial-time resolved UV–vis-NIR spectrometry, J. Catal. 352 (2017) 218–228.
[33] M.F. Baidoo, E. Fenes, K.R. Rout, T. Fuglerud, D. Chen, On the effects of K and La co-promotion on $CuCl_2$/γ-Al_2O_3 catalysts for the oxychlorination of ethylene, Catal. Today 299 (2018) 164–171.
[34] H. Ma, E. Fenes, Y. Qi, Y. Wang, K.R. Rout, T. Fuglerud, D. Chen, Understanding of K and Mg co-promoter effect in ethylene oxychlorination by operando UV–vis-NIR spectroscopy, Catal. Today (2020), https://doi.org/10.1016/j.cattod.2020.06.049.
[35] Y. Qi, E. Fenes, H. Ma, Y. Wang, K. Ranjan Rout, T. Fuglerud, M. Piccinini, D. Chen, Origin of potassium promotion effects on $CuCl_2$/γ-Al_2O_3 catalyzed ethylene oxychlorination, Appl. Surf. Sci. 521 (2020) 146310.
[36] N.B. Muddada, T. Fuglerud, C. Lamberti, U. Olsbye, Tuning the activity and selectivity of $CuCl_2$/γ-Al_2O_3 ethene oxychlorination catalyst by selective promotion, Top. Catal. 57 (2014) 741–756.
[37] R.V. Carrubba, J.L. Spencer, Kinetics of oxychlorination of ethylene, Ind. Eng. Chem. Proc. Des. Dev. 9 (1970) 414–419.
[38] B. Zhong, J. Zhao, Kinetics of oxychlorination of ethylene over copper catalysts, Shiyou Huagong 4 (1985) 23–28.
[39] Y.M. Bakshi, A.I. Gelbshtein, E.I. Gelperin, M.P. Dmitrieva, A.G. Zyskin, Y. S. Snagovskii, Study of the mechanism and kinetics of additive oxychlorination of olefins. 5. Kinetic-model of the reaction, Kinet. Catal. 32 (1991) 663–672.
[40] F. Chen, Y. Yang, S. Rong, G. Chen, Studies on ethylene oxychlorination II. Reaction mechanism and kinetics, Shiyou Huagong 7 (1994) 421–425.
[41] S. Wachi, Y. Asai, Kinetics of 1,2-dichloroethane formation from ethylene and cupric chloride, Ind. Eng. Chem. Res. 33 (1994) 259–264.
[42] A. Montebelli, E. Tronconi, C. Orsenigo, N. Ballarini, kinetic and modeling study of the ethylene oxychlorination to 1,2-dichloroethane in fluidized-bed reactors, Ind. Eng. Chem. Res. 54 (2015) 9513–9524.
[43] Z. Vajglová, N. Kumar, K. Eränen, M. Peurla, D.Y. Murzin, T. Salmi, Ethene oxychlorination over $CuCl_2$/γ-Al_2O_3 catalyst in micro- and millistructured reactors, J. Catal. 364 (2018) 334–344.
[44] http://www.eurokin.org/wp-content/uploads/webtool/EUROKIN_fixed-bed_html.htm.
[45] H.A. Jakobsen, Chemical Reactor Modeling, Multiphase Reactive Flows, Springer, 2008.
[46] Y. Qi, E. Fenes, H. Ma, Y. Wang, K.R. Rout, T. Fuglerud, M. Piccinini, D. Chen, Cluster-size-dependent interaction between ethylene and $CuCl_2$ clusters supported via γ-alumina, J. Phys. Chem. C 124 (2020) 10430–10440.
[47] Y.-C. Xie, Y.-Q. Tang, Spontaneous monolayer dispersion of oxides and salts onto surfaces of supports: applications to heterogeneous catalysis, Adv. Catal. Elsevier (1990) 1–43.
[48] G. Leofanti, M. Padovan, M. Garilli, D. Carmello, G.L. Marra, A. Zecchina, G. Spoto, S. Bordiga, C. Lamberti, Alumina-supported copper chloride, J. Catal. 189 (2000) 105–116.